Cyclone–Anticyclone Asymmetry Concerning the Height of the Thermal and the Dynamical Tropopause

VOLKMAR WIRTH

Meteorological Institute, University of Munich, Munich, Germany

(Manuscript received 20 August 1999, in final form 12 May 2000)

ABSTRACT

The differences between upper-tropospheric cyclones and anticyclones are investigated regarding the height of the thermal and the dynamical tropopause. The problem is addressed in an idealized framework by analyzing axisymmetric balanced flows, which are characterized by a radial scale ΔR and a tropopause potential temperature anomaly $\Delta\theta$, where cyclones and anticyclones differ only by the sign of $\Delta\theta$. The height of the thermal tropopause significantly differs from the height of the dynamical tropopause unless the anomaly is shallow. There is a pronounced asymmetry in that the differences are much larger and more likely to occur in the case of cyclones. Two factors contribute to this asymmetry. First, for a given amplitude $|\Delta\theta|$, cyclones and anticyclones have different aspect ratios in geometric space; second, for a high-latitude winter scenario the critical lapse rate of the WMO thermal tropopause is asymmetric with respect to typical tropospheric and stratospheric lapse rates. Simulated station statistics regarding the height of the two tropopauses share essential qualitative features with similar statistics from observations. The asymmetry in the model sensitively depends on the lower-stratospheric lapse rate. Multiple tropopauses may greatly enhance the asymmetry.

1. Introduction

The tropopause is an important meteorological concept. It separates the troposphere from the stratosphere, that is, two volumes of air that differ significantly in various properties (Holton et al. 1995). Correspondingly, various different quantities can be used to define ''the tropopause.'' The choice of the most suitable definition depends on the question to be addressed. The different tropopauses are not necessarily located at the same altitude.

Traditionally, the ''thermal tropopause'' has been defined as the lowest level at which the vertical temperature gradient, $\partial T/\partial z$, exceeds the value -2 K km^{-1}, provided that the average $\partial T/\partial z$ between this level and all higher levels within 2 km does not fall below this value again (WMO 1957). The thermal tropopause focuses on the difference in static stability between stratosphere and troposphere. More recently the ''dynamical tropopause'' has become popular (Danielsen 1968; Hoskins et al. 1985; WMO 1986). It is defined through a specific value of potential vorticity (PV). The dynamical tropopause (unlike the thermal tropopause) is a material surface under conservative conditions, which is an advantage, for instance, when considering the exchange of mass or constituents across the tropopause (e.g., Wirth 1995b; Wirth and Egger 1999). Bethan et al. (1996, referred to as BVR96 hereafter) introduced the ''ozone tropopause'' by specifying thresholds on both the value and the gradient of the ozone mixing ratio. In the Tropics, other measures can be used to define a tropopause (see Highwood and Hoskins 1998).

The ozone and the dynamical tropopause can be expected to behave similarly when the situation is dominated by synoptic-scale conservative dynamics. In this case, both ozone mixing ratio and PV are materially conserved. In addition, both quantities feature a sharp positive vertical gradient at the respective tropopause. Not surprisingly, one generally observes a strong spatial correlation between ozone mixing ratio and PV in the lower stratosphere (Beekmann et al. 1994). This suggests that under these circumstances the zone tropopause can be considered as a proxy for the dynamical tropopause (cf. BVR96). The ozone tropopause can be determined from a single sounding at one particular station, which is a notable advantage in comparison with the dynamical tropopause.

Our study is motivated by the work of BVR96, who analyzed several hundred ozonesonde profiles from northern European stations. They found a striking asymmetry between the location of the thermal and the ozone tropopause, where the ozone tropopause was located below the thermal tropopause in most cases with an

Corresponding author address: Dr. Volkmar Wirth, Meteorological Institute, University of Munich, Theresienstrasse 37, 80333 Munich, Germany.
E-mail: volkmar@meteo.physik.uni-muenchen.de

average difference of some 800 m. Large differences in tropopause height were associated with indefinite tropopauses that were, in turn, often associated with upper-tropospheric cyclonic flow conditions. The majority of the (rare) occurrences of an ozone tropopause being located above the thermal tropopause was associated with anticyclonic flow in the upper tropopshere. Bethan et al. suggest that the observed asymmetries should have a dynamic origin, but they do not provide a more detalied analysis. We did a similar observational study using a 31-yr (1967–97) record of ozone sonde profiles from the observatory at Hohenpeißenberg (Lerke 1999). The results (not shown) indicate that there, too, the ozone tropopause is more likely to be located below the themal tropopause than above it, although the asymmetry is not quite as pronounced as in BVR96. Unfortunately, there is no unique best definition of the ozone tropopause, and the results somewhat depend on the choice of the threshold values used. Nevertheless, the asymmetry described above can certainly be regarded as real. In view of the close connection between the ozone and the dynamical tropopause, it appears likely that there is a similar asymmetry between the thermal and the dynamical tropopause.

The above considerations motivated us to study the relation between the dynamical and the thermal tropopause focusing on possible asymmetries between cyclones and anticyclones implied by purely conservative dynamics. This work builds on an earlier paper by the same author (Wirth 2000, referred to as W2000 hereafter), in which the aspect ratio of the PV anomaly was used as control parameter governing the partitioning of the PV anomaly into a thermal and a dynamical anomaly. In that study, the thermal tropopause was sharp and coincided with the dynamical tropopause for shallow anomalies. On the other hand, anomalies whose vertical to horizontal scale was of the order $f/N \approx 1/100$ (where f denotes the Coriolis parameter and N is the Brunt–Väisälä frquency) were characterized by an indistinct thermal tropopause that was located at a height significantly different from the height of the dynamical tropopause. There was an approximate *antisymmetry* between cyclonic and anticyclonic flow (see Fig. 4 in W2000) with the thermal tropopause being located above the dynamical tropopause for cyclonic conditions, and below the dynamical tropopause for anticyclonic conditions. In the light of these results it was speculated that the observed asymmetry of BVR96 might be due to a fundamental asymmetry in aspect ratio between cyclones and anticyclones.

Although the present work is carried through in an idealized framework similar to that in W2000, there are a few important differences. Our approach will be as follows. First, we specify an idealized upper-tropospheric PV distribution that is characterized by a radial scale ΔR and a tropopause potential temperature anomaly $\Delta\theta$. Assuming rotational symmetry about the vertical axis, the inversion problem is solved (Hoskins et al. 1985) to obtain the balanced wind and temperature associated with the PV anomaly. Both the thermal and the dynamical tropopause height are diagnosed and compared with each other. The whole exercise is repeated many times for different values of ΔR and $\Delta\theta$ thus collecting synthetic statistical information about the location of the two tropopauses. Except for the sign of $\Delta\theta$, cyclones and anticyclones are treated identically. This is equivalent to assuming a certain (anti)symmetry between cyclones and anticyclones concerning their generation mechanism, because similar values of $|\Delta\theta|$ correspond to similar meridional displacements during the formation (see section 2a below). As we shall see, there are, nevertheless, significant asymmetries between cyclones and anticyclones. They will be explained in the framework of the model. The crucial difference between the present study and W2000 lies in the fact that here we specify the amplitude of the anomaly in terms of tropopause potential temperature, while in W2000 it was specified in terms of vertical tropopause displacement. As a consequence, in the present study the aspect ratio of the anomaly is part of the solution and not given a priori. Not surprisingly, this enables differences between cyclonic and anticyclonic conditions.

The plan of the paper is as follows. In section 2 we explain our model and provide, in particular, the physical motivation for our method of PV specification. The results are presented in section 3. A number of sensitivity studies reported in section 4 will uncover additional effects with potential relevance. Finally, section 5 provides a summary, some discussion and our conclusions.

2. Model

Our model consists in the construction and analysis of a large number of idealized axisymmetric balanced states. The two key parameters characterizing each anomaly are the scale ΔR of the radial extension of the anomaly and the amplitude $\Delta\theta$ of the tropopause potential temperature anomaly.

a. PV specification: Technique and physical motivation

Our anomalies are meant to be the result of upper-tropospheric advection under purely conservative conditions. Conceptionally it is easiest to imagine, first, a simple background atmosphere whose tropopause potential temperature varies smoothly with horizontal distance s. Let this background state be locally disturbed by horizontal advection across the background gradients creating a local anomaly, and let this anomaly finally cut off and become purely axisymmetric. Let, furthermore, the scale of the final anomaly be small enough such that the f plane is a plausible approximation. Since both potential temperature and potential vorticity are materially conserved by assumption, the specification

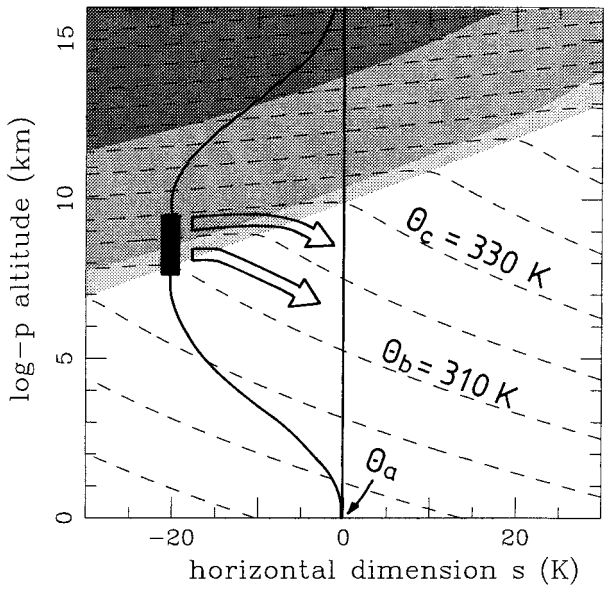

FIG. 1. Background atmosphere, which is used to construct the anomalies to be investigated. The dashed contours depict potential temperature $\theta(s, z)$ (in K, contours every 10 K), and the shading indicates potential vorticity $\hat{Q}(s, z)$ (in PVU, where 1 PVU = 10^{-6} $m^2\ s^{-1}\ K\ kg^{-1}$ and where the steps in shading are at 2, 4, and 8 PVU, with light shading representing low values and dark shading high values of PV). The vertical column at $s = -20$ K between $\theta_b = 310$ K and $\theta_c = 330$ K and the arrows indicate the construction of the anomaly invoking isentropic PV advection.

of the horizontal displacement Δs of each parcel on each isentrope determines the isentropic PV distribution of the final anomaly. Through PV inversion and transformation from potential temperature to height as the vertical coordinate, one eventually obtains all information necessary to diagnose the height of the different tropopauses. Note that this approach does not make any assumption about the vertical displacements occuring during the generation process; rather, they are predicted as part of the solution. The vertical displacements play a crucial role as they affect the location and sharpness of the different tropopauses in the final state. The latter too are predicted as part of the solution, which seems more desirable for the current investigation than specifying them a priori.

We first describe how we specify the background atmosphere (cf. Fig. 1). As an approximation to geometric altitude we use "log$p$ altitude" $z = -H \ln(p/p_o)$ as the vertical coordinate, where $H = 7$ km is a constant mean scale height, p denotes pressure, and $p_o = 1000$ hPa is a constant reference pressure (cf. Andrews et al. 1987). Horizontal distance is measured by a parameter s, which is defined as the deviation of the tropopause potential temperature θ^{tp} from a constant value $\theta_o^{\text{tp}} = 330$ K, that is,

$$\theta^{\text{tp}}(s) = \theta_o^{\text{tp}} + s. \tag{1}$$

The altitude z^{tp} of the nominal tropopause is taken to vary linearly with tropopause potential temperature θ^{tp} according to $z^{\text{tp}} = \theta_o^{\text{tp}} + A(\theta^{\text{tp}} - \theta_o^{\text{tp}})$, where $z_o^{\text{tp}} = 10$ km and $A = 10^{-1}$ km K^{-1} (cf. Juckes 1994). Furthermore, the vertical gradient T_z of the temperature T is taken as a piecewise constant with $T_z^{\text{trop}} = -6.5$ K km^{-1} in the troposphere and $T_z^{\text{strat}} = 0$ K km^{-1} in the stratosphere (and with a smooth transition between these constant values over a distance of a few hundred meters). This defines the thermal structure of the background atmosphere, expressed as temperature $\hat{T}(s, z)$ or potential temperature $\hat{\theta}(s, z) = \hat{T}(s, z)e^{\kappa z/H}$, respectively, where $\kappa = R/c_p$, R is the gas constant for dry air, and c_p is the specific heat at constant pressure. The corresponding distribution of potential vorticity $\hat{Q}$ (gray shading in Fig. 1) is computed as

$$\hat{Q}(s, z) = \frac{f(s)}{\rho_o}\frac{\partial \hat{\theta}}{\partial z}, \tag{2}$$

where $\rho_o(z) = p/(gH)$, where $g = 10$ m s^{-2} is the gravity acceleration, and where the contribution to PV of the relative vorticity is neglected (Andrews et al. 1987). The Coriolis parameter $f(s)$ is allowed to vary according to $f(s) = f_o(1 - Bs)$, with $f_o = 10^{-4}$ s^{-1} and $B = (60\ \text{K})^{-1}$. The parameter B introduces a variation of the background PV with the parameter s in the spirit of the β plane.

This background atmosphere is used to construct an axisymmetric PV distribution $Q(r, \theta)$ as follows (cf. Fig. 1). The undisturbed reference state is assumed to be motionless with $f = f_o$ and with the temperature profile corresponding to the background atmosphere at $s = 0$. Using radius r and potential temperature θ as coordinates, the PV distribution is defined as

$$Q(r, \theta) = \hat{Q}[\Delta s, \hat{z}(\Delta s, \theta)], \tag{3}$$

where $z = \hat{z}(s, \theta)$ is the inverse of $\theta = \theta(s, z)$. The quantity Δs can be interpreted as the amount of horizontal advection that has taken place during the formation of the anomaly. We set

$$\Delta s(r, \theta) = \Delta\theta \times \mathcal{C}(r; \Delta R) \times \mathcal{D}(\theta; \theta_a, \theta_b, \theta_c, \theta_d), \tag{4}$$

where $\Delta\theta$ is a constant amplitude; $\mathcal{C} = 1$ at $r = 0$ and smoothly goes to zero at $r = \Delta R$ in a $\cos^2$-like fashion; and $\mathcal{D} = 1$ for $\theta_b \le \theta \le \theta_c$ and smoothly blends to zero at θ_a and θ_d in, again, a $\cos^2$-like fashion. Here, $\theta_a = \hat{T}(0, 0)$ is the surface potential temperature, θ_b and θ_c are the lower and higher, respectively, of the background tropopause potential temperature at $s = 0$ and $s = \Delta\theta$, and $\theta_d = \theta_c + 100$ K. The "advection" is maximum (i.e., $\Delta s = \Delta\theta$) for the parcels in the tropopause region in the center of the anomaly and smoothly goes to zero above, below, and for larger radii. The resulting isentropic PV distributions for $\Delta R = 600$ km and $\Delta\theta = \pm 20$ K are shown in Fig. 2. As desired, our method yields an upper-tropospheric isentropic PV anomaly with a sharp vertical gradient corresponding to a well-defined dynamical tropopause, which is de-

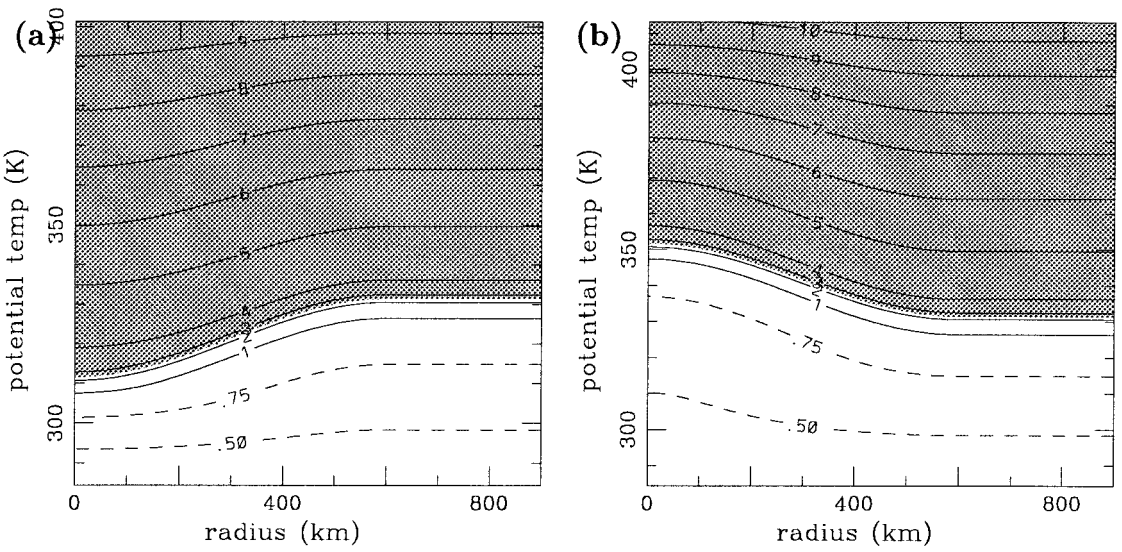

FIG. 2. Specified potential vorticity $Q(r, \theta)$ (contours, in PVU) corresponding to $\Delta R = 600$ km and $|\Delta\theta| = 20$ K. (a) Cyclonic anomaly ($\Delta\theta = -20$ K), (b) anticyclonic anomaly ($\Delta\theta = +20$ K). Gray shading indicates $Q \geq 2.5$ PVU. By definition, the dynamical tropopause is the interface between the white and the dark shaded regions. Only part of the computational domain is displayed.

fined through $Q = 2.5$ PV units (PVU) in this paper (1 PVU $= 10^{-6}$ m^2 s^{-1} K kg^{-1}).

b. PV inversion

Axisymmetric PV inversion on the f plane with potential temperature as the vertical coordinate is performed essentially as outlined in Hoskins et al. (1985). The PV is given by

$$Q = \frac{f + \tilde{\zeta}}{\sigma}, \tag{5}$$

where $\sigma = -g^{-1}\partial p/\partial\theta$ is density in isentropic coordinates, $\tilde{\zeta} = r^{-1}\partial(rv)/\partial r$ is the vertical component of relative vorticity in isentropic coordinates, and v is the tangential wind. One can derive the following equation:

$$\frac{\partial}{\partial r}\left[\frac{1}{r}\frac{\partial(rv)}{\partial r}\right] + \frac{Q}{g}\frac{\partial}{\partial\theta}\left(\frac{f_{\text{loc}}}{\mathcal{R}}\frac{\partial v}{\partial\theta}\right) = \sigma\frac{\partial Q}{\partial r}, \tag{6}$$

with $f_{\text{loc}} = f + 2v/r$ and $\mathcal{R}(p) = Rp_o^{-\kappa}p^{\kappa-1}$. The thermal wind equation reads

$$f_{\text{loc}}\frac{\partial v}{\partial\theta} = \mathcal{R}\frac{\partial p}{\partial r}. \tag{7}$$

For a given Q, (6) can be considered as a linear elliptic partial differential equation for v, provided $f_{\text{loc}}Q > 0$ and σ, f_{loc}, and $\mathcal{R}$ are known. However, the latter three quantities depend on v, either directly or indirectly via (7) and the definition of σ, so that (6) together with (7) must be regarded as a coupled nonlinear problem.

Integration of the thermal wind equation (7) proceeds inward from the outer boundary, where we specify $p(\theta)$ to be equal to the background atmosphere at $s = 0$. Regarding (6), we use the natural boundary condition $v = 0$ at $r = 0$, and we set $\partial(rv)/\partial r = 0$ at the outer boundary. This ensures that both the temperature profile and the PV profile at the outer boundary are equal to the corresponding reference profile, that is, the background profile at $s = 0$. At the upper and lower boundary we specify $\partial v/\partial\theta = 0$. This corresponds to zero temperature anomaly at the earth's surface and above the lower stratosphere implying a baroclinic formation mechanism for the tropopause anomaly. As discussed in W2000, one may expect some sensitivity to the lower boundary condition for shallow anomalies. On the other hand, the asymmetries which we focus on in this paper are associated with intermediate and tall anomalies, suggesting that our results do not sensitively depend on the choice of these boundary conditions.

The PV inversion is performed numerically on a domain extending from $\theta = \theta_a$ to $\theta_d + 150$ K in the vertical, and from $r = 0$ to $3\Delta R/2$ in the radial direction. The equations are discretized using standard finite differences on a grid with 67 and 259 grid points in the horizontal and vertical, respectively. The problem is solved iteratively as outlined in Hoskins et al. (1985) using a multigrid algorithm from the Numerical Algorithms Group. Convergence is monitored through a norm on v. The iteration is terminated when the relative difference between successive iterations is less than 0.1%, which typically requires between 10 and 20 iterations. The accuracy of the algorithm was tested by comparing the PV distribution calculated from the wind and temperature with the original PV distribution. The maximum difference was found to be around 0.2 PVU. This translates to a maximum error for the height of the

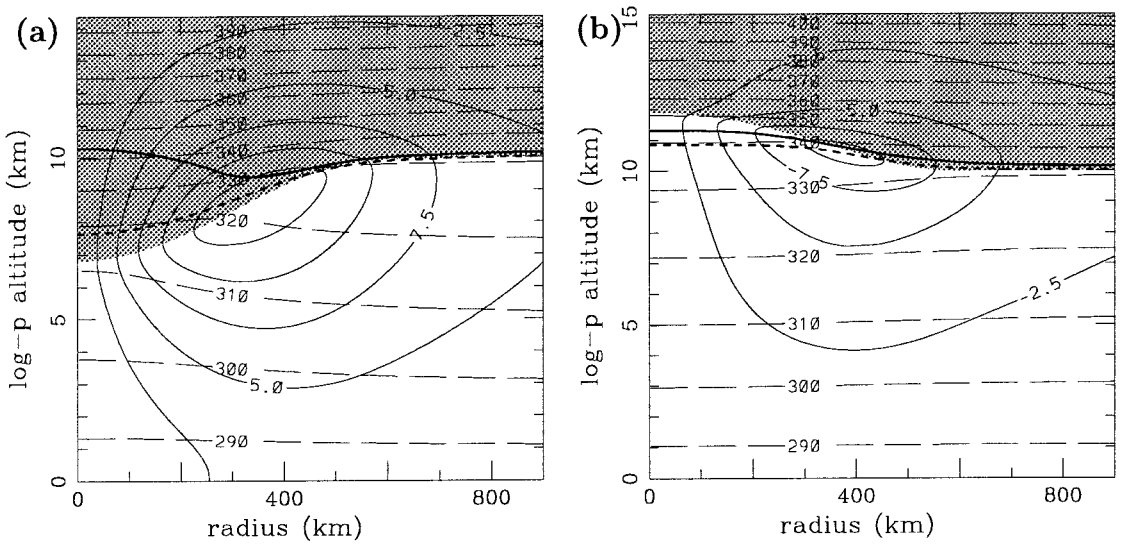

FIG. 3. Two axisymmetric balanced states corresponding to the PV distributions of Fig. 2, i.e., $\Delta R = 600$ km and $|\Delta\theta| = 20$ K. Here, the fields are ploted as a function of radius r and altitude z. (a) Cyclonic anomaly ($\Delta\theta = -20$ K), (b) anticyclonic anomaly ($\Delta\theta = +20$ K). In both panels, the solid contours depict tangential wind v (in m s^{-1}, contours every 2.5 m s^{-1}) and the dashed contours potential temperature θ (in K, contours every 10 K). Gray shading indicates $Q \geq 2.5$ PVU. By definition, the dynamical tropopause is the interface between the white and the dark shaded regions. The thick solid line is the thermal tropopause, and the thick dashed line is the modified thermal tropopause, i.e., the location where the lapse rate is midway between the reference tropospheric and stratospheric lapse rates. Only part of the computational domain is displayed.

dynamical tropopause of some 100 m, which is certainly accurate enough for the current application.

Finally, the fields are transformed to make them functions of radius r and height z, that is,

$$\tilde{T}(r, z) = T[r, \theta(r, z)], \tag{8}$$

and similarly for v and Q. The inversion is performed numerically. The final states corresponding to the PV distributions of Fig. 2 are displayed in Fig. 3.

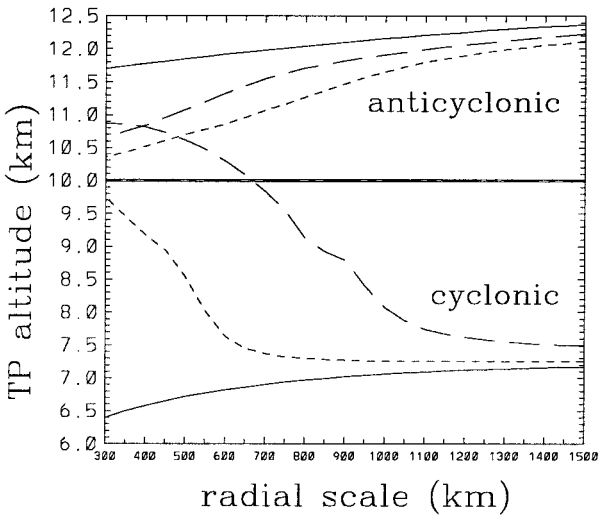

FIG. 4. Tropopause height in the center of the anomaly as a function of the radial-scale parameter ΔR for anomalies with fixed amplitude $|\Delta\theta| = 20$ K. The thin solid lines represent the dynamical tropopause, the long dashes the thermal tropopause, and the short dashes the modified thermal tropopause. The upper curves represent anticyclonic, the lower curves cyclonic anomalies. The thick solid line marks the height z^{tp}_{ref} of the reference tropopause.

3. Results

For the computation of the thermal tropopause we implemented the World Meteorological Organization (WMO) definition as given in the introduction. The dynamical tropopause is defined through the threshold $Q = 2.5$ PVU.

a. Tropopause height in the center of the anomaly

First we produce a large number of anomalies with the amplitude kept fixed at $|\Delta\theta| = 20$ K while varying the radial-scale parameter ΔR between 300 and 1500 km. The two thin solid lines in Fig. 4 show the height z^{tp}_{dyn} of the dynamical tropopause in the center of the anomaly as a function of ΔR. There is a pronounced asymmetry between cyclonic (lower line) and anticyclonic (upper line) anomalies, which increases as the radial scale ΔR decreases. At $\Delta R = 300$ km the displacement of the dynamical tropopause from its reference position z^{tp}_{ref} (=10 km, thick solid line) is almost 3 times larger for the cyclonic than for the anticyclonic anomaly. Formally, this asymmetry is a consequence of the nonlinearity of the equations. In more physical terms, the asymmetry can be viewed as a result of the vertical wind that accompanies the horizontal-scale contraction during the implied formation of the anomaly.

As was shown in W2000, the vertical wind systematically deepens the PV anomaly in the cyclonic case but makes it flatter in the anticyclonic case.

The height $z^{\rm tp}_{\rm therm}$ of the thermal tropopause in the center of the anomaly is plotted with long dashes in Fig. 4. As in W2000, the thermal tropopause is located above the dynamical tropopause for cyclones and below the dynamical tropopause for anticyclones, but now there is a pronounced asymmetry between cyclones and anticyclones. For cyclones, the difference between the two tropopauses is up to a factor 4 larger (when $\Delta R \lesssim 500$ km). In addition, significant deviations between the two tropopauses appear in a broader range of values of ΔR.

The asymmetry between cyclones and anticyclones concerning the height difference $\Delta z^{\rm tp} = z^{\rm tp}_{\rm therm} - z^{\rm tp}_{\rm dyn}$ between the two tropopauses can be interpreted in terms of the results of W2000. Anomalies with a small value of ΔR are ''tall'' anomalies for which the temperature perturbation is relatively weak. In the limit $\Delta R \to 0$ (while keeping $\Delta\theta$ fixed) the isentropes in Fig. 3 would, pictorially speaking, become purely horizontal with their positions determined by the reference profile at the outer boundary, while the PV–θ relation would remain unchanged. It is, thus, essentially the difference of the vertical gradient of the reference potential temperature profile $\theta_{\rm ref}(z)$ between troposphere and stratosphere that allows the PV anomaly to become rather deep in the cyclonic case ($z^{\rm tp}_{\rm dyn} - z_{\rm ref} \to -4.61$ km, for $\Delta R \to 0$) but much less deep in the anticyclonic case ($z^{\rm tp}_{\rm pv} - z_{\rm ref} \to +1.61$ km, for $\Delta R \to 0$). To remove this obvious asymmetry we define the normalized altitude difference by dividing the actual difference $\Delta z^{\rm tp}$ by its theoretical value $\Delta z^{\rm tp}_o$ in the limit $\Delta R \to 0$. Furthermore, instead of ΔR, we use as control parameter the aspect ratio, defined as

$$\mathcal{A} = 100\frac{|z^{\rm tp}_{\rm dyn} - z_{\rm ref}|}{\Delta R}, \tag{9}$$

where the factor 100 is taken as representative for N/f. Indeed, the result (long dashes in Fig. 5) shows an approximate, albeit not perfect, symmetry between cyclones and anticyclones. This result suggests that a substantial portion of the asymmetry of $\Delta z^{\rm tp}$ in Fig. 4 arises from the fact that for given values of ΔR and $\Delta\theta$ the cyclonic anomaly has a larger dynamical tropopause anomaly and, as a consequence, a taller aspect ratio than the corresponding anticyclonic anomaly. However, as we shall later see, the approximate symmetry for the thermal tropopause in Fig. 5 is somewhat fortuitous.

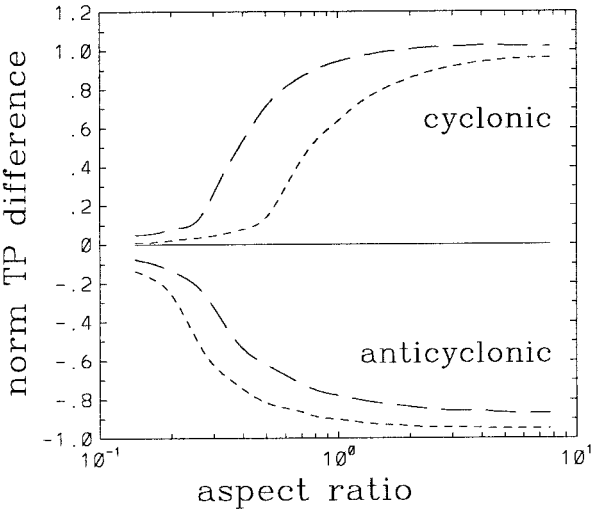

FIG. 5. Normalized altitude difference $\Delta z^{\rm tp}/\Delta z^{\rm tp}_o$ between the thermal and the dynamical tropopause in the center of the anomaly for anomalies with fixed amplitude $|\Delta\theta| = 20$ K, but varying horizontal-scale parameter ΔR, plotted as a function of the aspect ratio $\mathcal{A}$. The long dashes represent the thermal tropopause and the short dashes the modified thermal tropopause. The upper curves represent cyclonic, the lower curves anticyclonic anomalies. The zero line is indicated by a straight solid line.

b. Tropopause–tropopause scatterplots

Next we produce synthetic statistical information in the framework of our model. To this end we consider M^2 different cyclonic and M^2 different anticyclonic anomalies by systematically varying the two parameters ΔR and $|\Delta\theta|$ according to $\Delta R_i = \Delta R_{\rm min} + (i-1)(\Delta R_{\rm max} - \Delta R_{\rm min})/(M-1)$, $i = 1, 2, \ldots, M$, and $\pm\Delta\theta_j = \Delta\theta_{\rm min} + (j-1)(\Delta\theta_{\rm max} - \Delta\theta_{\rm min}/(M-1)$, $j = 1, 2, \ldots, M$, with $\Delta R_{\rm min} = 300$ km, $\Delta R_{\rm max} = 1500$ km, $\Delta\theta_{\rm min} = 5$ K, and $\Delta\theta_{\rm max} = 20$ K. In addition, the tropopause height $z^{\rm tp}_{\rm ref}$ of the reference atmosphere at the outer boundary is randomly varied between 9 km $\le z^{\rm tp}_{\rm ref} \le$ 11 km according to an equal distribution. The latter device avoids spurious correlations and is easily implemented through adding s_o to the right-hand side of (4), with s_o varying between -10 and $+10$ K according to an equal distribution. It can be interpreted as simulating variations of the unperturbed tropopause height due to, for instance, the seasonal cycle or other factors that are not accounted for explicitly in our model. Each anomaly thus obtained is analyzed at K different radii $r_k = (k-1)\Delta R/(K-1)$, $k = 1, 2, \ldots, K$. This method yields $N = 2KM^2$ different profiles with information about the height of the two tropopauses. The whole procedure is meant to simulate a large number of profiles encountered by a station at a fixed geographical location. Because the primary focus of this study is the asymmetry between cyclones and anticyclones, no attempt is made to simulate realistic statistical distributions for ΔR_i, $\Delta\theta_j$, and r_k. We choose $M = 10$ and $K = 5$, which gives us a total of $N = 1000$ profiles.

The mean difference $\langle\Delta z^{\rm tp}\rangle \equiv N^{-1}\sum_{i=1}^{N}(z^{\rm tp}_{{\rm therm},i} - z^{\rm tp}_{{\rm dyn},i})$ between the thermal and the dynamical tropopause for all $N = 1000$ profiles is $+275$ m. This single number quantifies the cyclone–anticyclone asymmetry in a broad sense, as one would expect $\langle\Delta z^{\rm tp}\rangle = 0$ in a perfectly symmetric situation. Since the cyclone–anticyclone asymmetry is our main focus, this run and all further runs (to be described later) are summarized and

TABLE 1. Mean height difference $\langle \Delta z^{tp} \rangle$ (in m) between thermal and dynamical tropopause. This mean height difference quantifies in a broad sense the cyclone–anticyclone asymmetry in the current context. The different columns correspond to the different experiments described in this paper. In each column, the first row gives $\langle \Delta z^{tp} \rangle$ computed from all profiles, while rows 2–4 refer to subsamples containing the sharp, intermediate, and indefinite thermal tropopauses.

	Control	Less stable	More stable	Multiple TP	Second sample	Second sample, less stable	Second sample, more stable
All	275	511	188	772	534	909	348
Sharp	−5	13	−14	120	−43	−46	−25
Intermediate	126	181	107	729	79	165	16
Indefinite	708	1347	475	1473	1572	2625	1057

compared to each other in terms of $\langle \Delta z^{tp} \rangle$ in Table 1. In this table, the control run discussed at this point appears as the first column.

The corresponding scatterplot is shown in Fig. 6a, where each symbol represents one profile. Note that in this plot (and all subsequent plots of this kind) only those profiles are included that satisfy $|\Delta z^{tp}| \geq 0.5$ km. Of these, 130 have the thermal tropopause above the dynamical tropopause, while the opposite is true for only 16. The strong asymmetry in Fig. 6a is qualitatively very much like the asymmetry in BVR96, although in the latter study the mean difference for all profiles was significantly larger (some 800 m). Figure 6a distinguishes between cyclonic (circles) and anticylonic (squares) anomalies showing that all profiles with $\Delta z^{tp} \geq 0.5$ km are associated with cyclonic anomalies, while all profiles with $\Delta z^{tp} \leq -0.5$ km are associated with anticyclonic anomalies—again in qualitative agreement with the corresponding results of BVR96.

We classify the profiles according to the sharpness of the thermal tropopause (cf. Price and Vaughan 1993; BVR96). To this end we consider the change in lapse rate over a distance of 1 km centered about the thermal tropopause. Three classes (sharp, intermediate, and indefinite) are introduced with the respective boundaries defined such that an (almost) equal number of profiles falls into each of them. It turns out that all profiles plotted in Fig. 6a belong to the class of the indefinite thermal tropopause. Similarly, the mean height difference Δz^{tp} computed separately for the three different classes (second through fourth row in Table 1) indicates the tendency for substantially larger deviations in the case of a less definite tropopause. Again, these findings are in qualitative agreement with BVR96.

c. *Asymmetry in the definition of the WMO thermal tropopause*

The thermal tropopause is defined through the WMO criterion involving the critical lapse rate $T_z^{wmo} = -2$ K km^{-1}. In view of our idealized reference atmosphere with a piecewise constant lapse rate ($T_z^{trop} = -6.5$ K km^{-1} in the troposphere and $T_z^{strat} = 0$ K km^{-4} in the stratosphere), the critical lapse rate T_z^{wmo} is closer to the stratospheric than to the tropospheric lapse rate. It is hypothesized that this fact is at least partly responsible for the asymmetries found above. To test this hypothesis, we introduce a ''modified thermal tropopause'' through

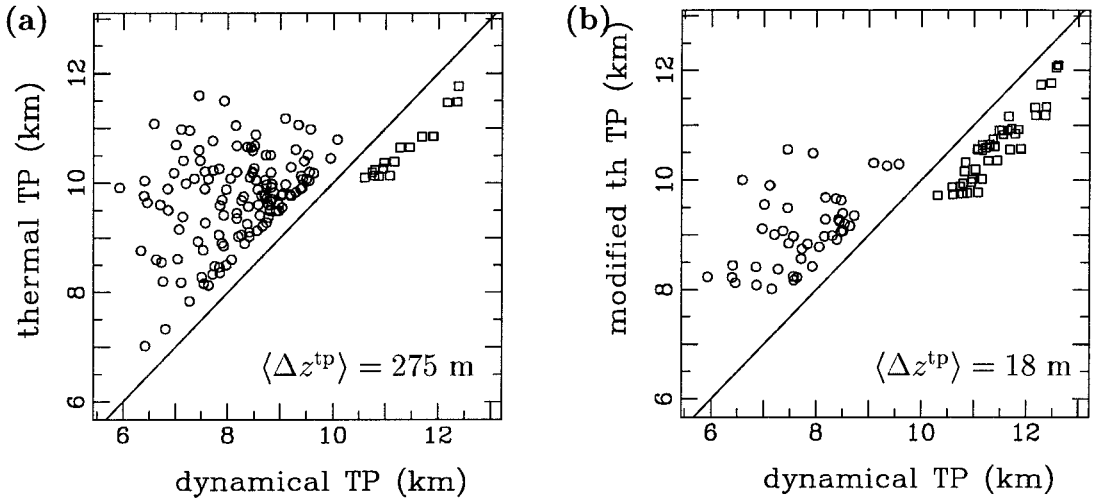

FIG. 6. Scatterplot of the height of the thermal tropopause vs the height of the dynamical tropopause, (a) for the conventional WMO thermal tropopause, and (b) for the modified thermal tropopause. Only profiles with $|\Delta z^{tp}| \geq 0.5$ km are entered in this diagram. Circles represent profiles from cyclonic, squares profiles from anticyclonic anomalies. The average difference $\langle \Delta z^{tp} \rangle$ of all profiles (not only the displayed ones) is given in the lower right corner of each panel.

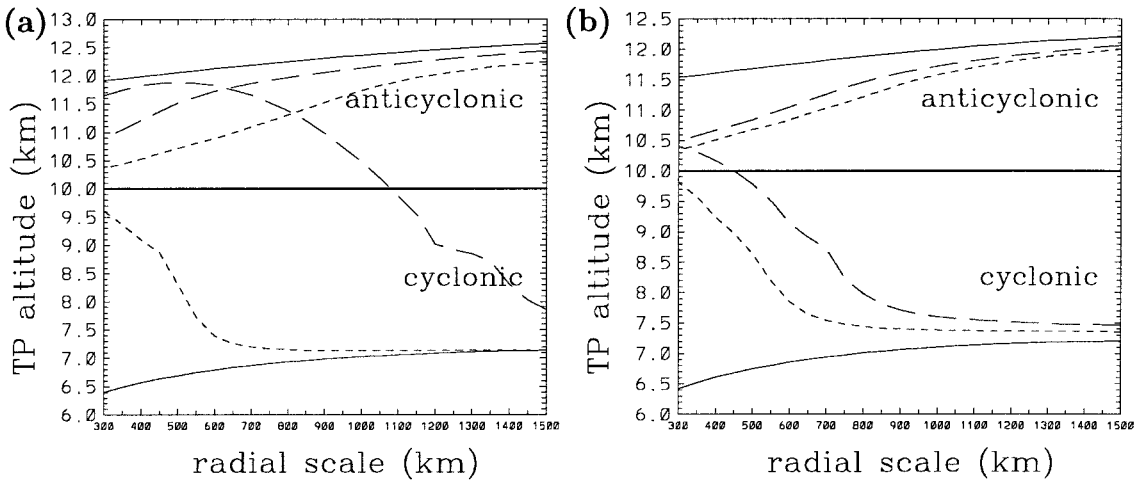

FIG. 7. As in Fig. 4, but for the experiments with a modified stratospheric lapse rate in the reference atmosphere. (a) $T_z^{\text{strat}} = -1$ K km^{-1}, and (b) $T_z^{\text{strat}} = +1$ K km^{-1}.

a threshold value $T_z^{\text{mod}} = (T_z^{\text{trop}} + T_z^{\text{strat}})/2$, lying halfway between the reference tropospheric and stratospheric lapse rates.

Not surprisingly, the modified thermal tropopause lies consistently below the WMO thermal tropopause (thick dashed line in Fig. 3 and short dashes in Fig. 4). The modification has a substantial impact on the behavior in Fig. 4, and part of the asymmetry is lost. Similarly, the behavior of the modified thermal tropopause in Fig. 5 (short dashes) differs from the behavior of the WMO thermal tropopause. Interestingly, significant deviations appear at smaller values of the aspect ratio in the anticyclonic case, rendering the behavior of the modified tropopause in this diagram *less* symmetric than that of the WMO thermal tropopause. This suggests that the approximate symmetry for the WMO tropopause noted in connection with Fig. 5 (as in W2000) is somewhat fortuitous, as it depends on the asymmetric nature of the WMO definition.

The scatterplot for the modified thermal tropopause (Fig. 6b) shows 45 profiles with $\Delta z^{\text{tp}} \geq 0.5$ km and 43 profiles with $\Delta z^{\text{tp}} \leq -0.5$ km. The average difference is $\langle \Delta z^{\text{tp}} \rangle = 18$ m. Thus, in a broad sense the situation is much more symmetric for the modified thermal tropopause than for the usual thermal tropopause, even though certain asymmetries remain (e.g., the different spread of the points displayed in the scatterplot; see also the different behavior of the short dashes in Fig. 4).

In summary, part of the asymmetry in our model between the thermal and the dynamical tropopause is due to the fact that the critical lapse rate in the WMO definition is closer to a typical stratospheric lapse rate than to a typical tropospheric lapse rate.

4. Sensitivities

We performed an extensive set of experiments to study the sensitivity of our results with respect to various assumptions and parameters. In most cases the essence of the results presented in the previous section remained qualitatively unchanged. In the following, only experiments revealing large and potentially relevant effects will be reported.

a. Stratospheric static stability

The asymmetry of the WMO thermal tropopause critical lapse rate with respect to the tropospheric and the stratospheric lapse rate of our background atmosphere suggests that there must be a significant sensitivity to the lower-stratospheric static stability. For instance, when $T_z^{\text{strat}} \gtrsim -2$ K km^{-1} (rather than $T_z^{\text{strat}} = 0$ K km^{-1}, as in our control experiment), a small amount of destabilization through horizontal-scale contraction during the formation of a cyclonic anomaly suffices to render lower-stratospheric air tropospheric regarding the WMO thermal tropopause. On the other hand, when the reference lower stratosphere is more stable (e.g., $T_z^{\text{strat}} = +1$ K km^{-1} or $+2$ K km^{-1}), the WMO thermal tropopause more closely corresponds to our modified thermal tropopause, and one can expect a more symmetric behavior. To quantify the sensitivity we repeated the model runs with $T_z^{\text{strat}} = -1$ K km^{-1} (less stable stratosphere) and $T_z^{\text{strat}} = +1$ K km^{-1} (more stable stratosphere), respectively.

The modification leaves the wind field obtained from the PV inversion almost unchanged (not shown). Similarly, the location of the dynamical tropopause is affected only marginally, as can be inferred from the solid lines in Fig. 7. On the other hand, the thermal tropopause shows a considerably more pronounced deviation from the dynamical tropopause for the less stable stratosphere (Fig. 7a, long dashes vs solid lines) in comparison with the control experiment (Fig. 4). Note that in the cyclonic case the thermal tropopause is located even above the reference tropopause over a wide range of values of ΔR.

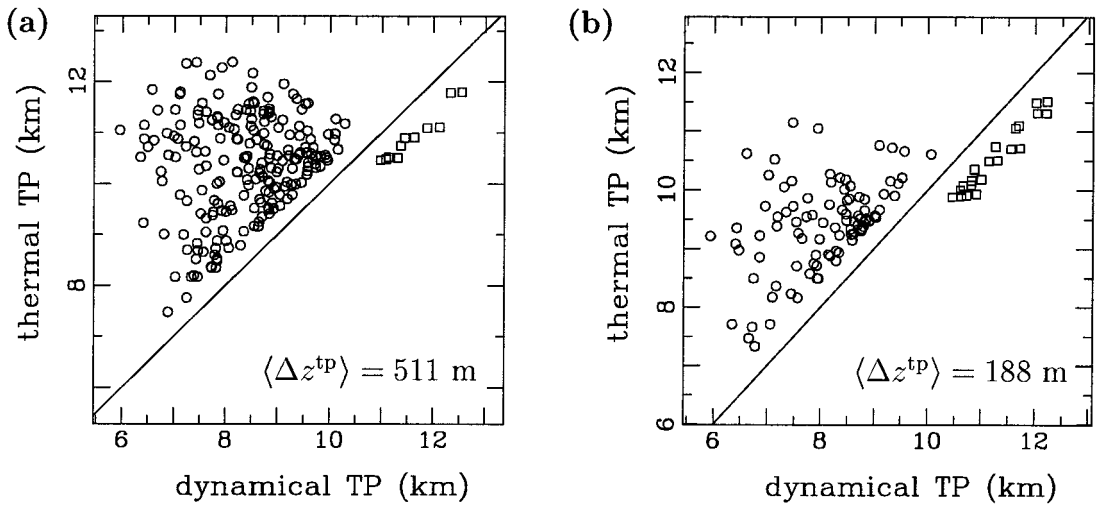

FIG. 8. As in Fig. 6a, but for the experiments with a modified stratospheric lapse rate in the reference atmosphere. (a) $T_z^{\text{strat}} = -1$ K km^{-1}, and (b) $T_z^{\text{strat}} = +1$ K km^{-1}.

Reversely, the deviation is less pronounced for the more stable stratosphere (Fig. 7b). The modified thermal tropopause (short dashes) is only marginally affected by the change in stratospheric lapse rate, indicating that the strong sensitivity for the WMO thermal tropopause is predominantly due to the asymmetry of the lapse rate criterion. Plotting the normalized tropopause difference as a function of aspect ratio (not shown) reveals, again, that the approximate symmetry for the thermal tropopause in Fig. 5 is fortuitous, as it sensitively depends on the lower-stratospheric lapse rate.

The scatterplots, too, are strongly sensitive to the lower stratospheric lapse rate (Fig. 8). In the case of the less stable stratosphere (Fig. 8a), one obtains a mean tropopause difference of $\langle \Delta z^{\text{tp}} \rangle = 511$ m, which is almost twice as much as in the control run, and there are significantly more profiles with $\Delta z^{\text{tp}} \geq 0.5$ km than in the control run (207 here vs 130 in Fig. 6a). The change is somewhat less dramatic in the case of the more stable stratosphere (Fig. 8b), where the mean tropopause difference is $\langle \Delta z^{\text{tp}} \rangle = 188$ m with 93 profiles having $\Delta z^{\text{tp}} \geq 0.5$ km. The second and third columns in Table 1 show that the tendency of less definite thermal tropopauses to be related to larger mean differences $\langle \Delta z^{\text{tp}} \rangle$ is qualitatively as in the control experiment, although the absolute numbers differ significantly.

b. Filaments and multiple tropopauses

So far we only considered anomalies with a unique tropopause (both dynamical and thermal). However, in the real atmosphere one often encounters multiple tropopauses. For instance, the formation of a strong upper-tropospheric cyclone is sometimes accompanied by a so-called tropopause fold (Shapiro 1980). Regarding the smaller scales, filaments of stratospheric air have been observed in the upper troposphere, and vice versa (Dobson 1973; Reid and Vaughan 1991). We, therefore, investigated how our results are modified in the presence of multiple tropopauses.

In order to simulate a scenario with multiple tropopauses, we replace r on the right-hand side of (4) by $r_{\text{mod}}(r, \theta) = \max[0, r - g(\theta)\Delta R]$, where $g(\theta_o) = 1$ (with $\theta_o = \theta_b$ for cylcones and $\theta_o = \theta_c$ for anticyclones) and where $g(\theta)$ smoothly goes to zero away from θ_o. Pictorially speaking, filaments are generated by drawing air outward from the center of the anomaly in the region of that isentropic level that corresponds to the maximum tropopause anomaly. The resulting balanced states for $\Delta R = 1000$ km and $\Delta\theta = \pm 20$ K are displayed in Fig. 9. There is a noticeable asymmetry between the cyclonic and the anticyclonic case. For the cyclonic anomaly, the filament which is ''drawn outward'' during the assumed generation process follows the downward slope of the ambient isentropes, resulting in a rather large displacement of the filament away from the ''main'' tropopause (the main tropopause is the dynamical tropopause in the absence of the filament). Similarly, the air is drawn outward and (slightly) downward in the case of the anticylonic anomaly, but now this results in the filament being rather close to the main tropopause.

There is yet another relevant issue. The WMO thermal tropopause requires the lapse rate criterion to be satisfied in an average sense over a depth of 2 km. The dynamical tropopause, on the other hand, does not involve a similar requirement. As a consequence, the thermal tropopause is likely to be diagnosed at a higher position than the dynamical tropopause in the presence of a thin filament. This effect is independent of the sense of the anomaly and thereby introduces another source for cyclone–anticyclone asymmetry.

Both effects combine. The resulting impact is large, as demonstrated in Fig. 10 where a large number of profiles (397 out of 1000) have $\Delta z^{\text{tp}} \geq 0.5$ km. The

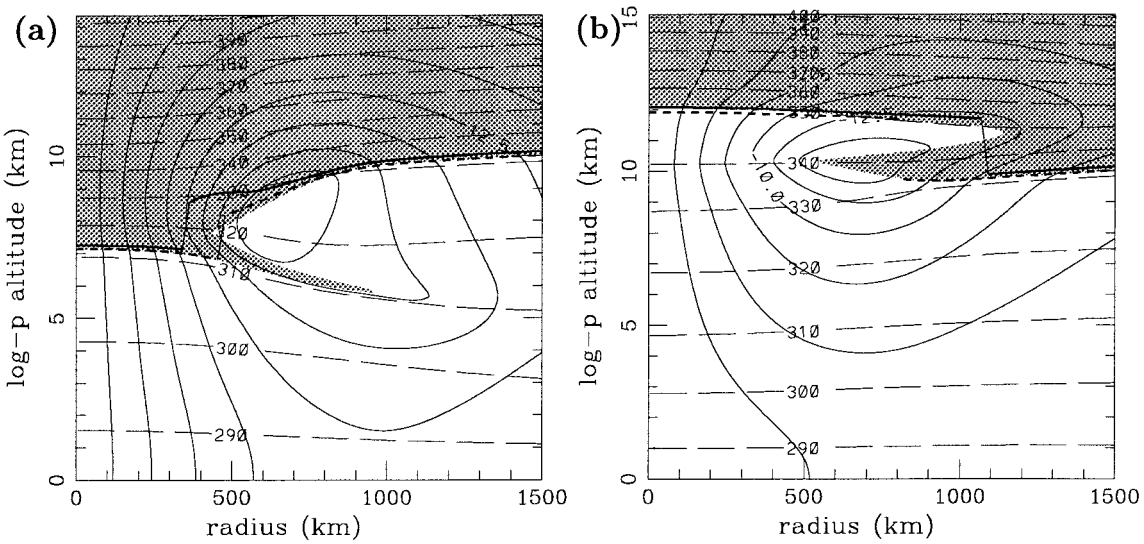

FIG. 9. As in Fig. 3, but with $\Delta R = 1000$ km and modified to obtain multiple dynamical tropopauses.

average difference is $\langle \Delta z^{\rm tp} \rangle = 772$ m, which is much larger than in the control case (see Table 1). Note that here, as opposed to the control experiment, even anticyclonic profiles yield $\Delta z^{\rm tp} \geq 0.5$ km. The tendency for larger mean deviations $\langle \Delta z^{\rm tp} \rangle$ in the case of less definite tropopauses (fourth column in Table 1) is, again, qualitatively like in the control experiment.

c. Impact of the vortex sample on the scatterplot

Naturally, the quantitative information contained in our tropopause–tropopause scatterplots sensitively depends on the chosen sample of anomalies. As can be inferred from Fig. 4, a sample with a relatively small mean $\langle \Delta R \rangle$ is likely to have a relatively large mean tropopause difference $\langle \Delta z^{\rm tp} \rangle$, and vice versa. For instance, halving the value of $\Delta R_{\rm max}$ and doubling the value of $\Delta\theta_{\rm min}$ (i.e., $\Delta R_{\rm max} = 750$ km and $\Delta\theta_{\rm min} = 10$ K) yields $\langle \Delta z^{\rm tp} \rangle = 534$ m, which is almost twice as large as in the control run (fifth column in Table 1, denoted as ''second sample''). On the other hand, the essential qualitative features remain unchanged. As before, reference to the modified thermal tropopause rather than the WMO thermal tropopause substantially reduces the mean tropopause difference (yielding $\langle \Delta z^{\rm tp} \rangle = 71$ m). A less stable stratosphere ($T_z^{\rm strat} = -1$ K km^{-1}) substantially increases the mean difference to $\langle \Delta z^{\rm tp} \rangle = 909$ m, while a more stable stratosphere ($T_z^{\rm strat} = +1$ K km^{-1}) decreases this value to $\langle \Delta z^{\rm tp} \rangle = 348$ m (Table 1, columns 6 and 7). Similarly, the overall tendency for larger deviations $\langle \Delta z^{\rm tp} \rangle$ in the case of less definite tropopauses is, again, as in the control experiment (see Table 1).

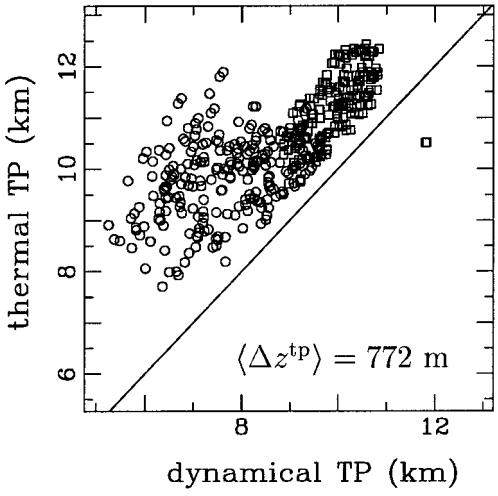

FIG. 10. As in Fig. 6a, but for anomalies with multiple dynamical tropopauses.

5. Summary, discussion, and conclusions

In this study, we investigated asymmetries between upper-tropospheric cyclones and anticyclones regarding the height of the thermal and the dynamical tropopause. The problem was addressed in an idealized framework involving axisymmetric isentropic PV inversion of anomalies, which are characterized by a radial scale ΔR and a tropopause potential temperature anomaly $\Delta\theta$. Anticyclones differ from their cyclonic counterparts only by the sign of $\Delta\theta$. This corresponds to assuming a certain symmetry between cyclones and anticyclones regarding their formation. The model should have relevance for the real atmosphere if, and to the degree that, real anomalies arise through the action of conservative balanced dynamics involving substantial horizontal-scale contraction, and there is an approximate symmetry between cyclones and anticyclones concerning their amplitude $|\Delta\theta|$.

For the same reasons as in W2000, the height of the thermal tropopause significantly differs from the height of the dynamical tropopause unless the anomaly is shallow. However, the current model uncovers a pronounced asymmetry between cyclones and anticyclones. In the case of cyclones, one obtains much larger differences $|\Delta z^{\text{tp}}|$ between the thermal and the dynamical tropopause than for anticyclones. In addition, substantial differences between the two tropopauses are more likely as they occur in a broader range of radial scales. These asymmetries were found to be related to a combination of two factors. First, for given values of ΔR and $|\Delta\theta|$, cyclones have taller aspect ratios than anticyclones; second, the critical lapse rate of the WMO thermal tropopause is closer to the stratospheric than the tropospheric lapse rate of the model reference atmosphere.

We tried to relate our results to the observations of BVR96. For this purpose large samples of anomalies were produced covering a whole range of values of both ΔR and $\Delta\theta$. From these anomalies profiles were extracted at various radii, providing us with simulated tropopause statistics at a specific observation site. Accepting the observed ozone tropopause as a proxy for the dynamical tropopause, our statistics can be compared with those of BVR96. We found good qualitative agreement regarding several essential features. In both, the average thermal tropopause is above the average dynamical (or ozone, respectively) tropopause; the thermal tropopause is rather indefinite in the case of a large tropopause difference; and the (rare) occurrences of a thermal tropopause below the dynamical (ozone) tropopause are associated with anticyclonic conditions.

It would be easy to simulate an ozone tropopause in our model. Indeed, we did this by specifying an idealized distribution of ozone mixing ratio χ in our reference atmosphere with $\partial\chi/\partial z = 0$ in the troposphere and $\partial\chi/\partial z = \chi_{oz} = \text{const} > 0$ in the stratosphere. The anomaly of the ozone mixing ratio was constructed in the same way as the PV anomaly, consistent with the assumption that both PV and ozone mixing ratio are materially conserved on the timescales considered. Defining the ozone tropopause through a critical value of χ allows one to make the ozone tropopause essentially equivalent to the dynamical tropopause, since both are material surfaces. However, we also found good agreement between the two tropopauses even when the ozone tropopause is defined through a critical value χ_z^{crit} on the ozone mixing ratio vertical gradient, as long as this critical value is well separated from χ_{oz}. In that case, even though vortex stretching changes the vertical gradient $\partial\chi/\partial z$, this change is not sufficient to make the ozone tropopause deviate substantially from a material surface, because the ozone tropopause is always located at the kink in the ozone mixing ratio profile. Thus, with reasonable assumptions about the reference ozone distribution and a suitable definition of the ozone tropopause, the latter is practically equivalent to the dynamical tropopause in our model.

There is strong sensitivity to the lower-stratospheric lapse rate with a less stable stratosphere leading to an enhanced asymmetry. This sensitivity was shown to be related to the asymmetry of the definition of the WMO thermal tropopause with respect to typical tropospheric and stratospheric lapse rates. Because in winter the lower stratosphere is generally less stable in polar latitudes than in midlatitudes or the subtropics (e.g., Defant and Taba 1957), one may expect particularly strong asymmetries at higher latitudes. In this context it is relevant to note that all the data used in BVR96 stem from mid- and northern European stations during winter and early spring. Their strong asymmetry may, therefore, be partly due to the asymmetry of the WMO definition of the thermal tropopause.

In the case of multiple tropopauses the amount of asymmetry sensitively depends on whether or not the definition of the dynamical tropopause involves a criterion on the minimum stratospheric layer depth. If there is no such criterion, the dynamical tropopause is likely to be at a lower altitude than the thermal tropopause for both cyclones and anticyclones, which results in a larger mean tropopause height difference. This sensitivity must be kept in mind when comparing the observations of BVR96 with our results. It suggests that part of the asymmetry in BVR96 arises because they did not require a minimum stratospheric layer depth in their definition of the ozone tropopause.

There are also nondynamical factors that result in differences between cyclones and anticyclones, like for instance the asymmetry due to diabatic processes pointed out by Hoskins et al. (1985). For cyclonic anomalies one may expect strong diabatic processes involving the release of latent heat (Wirth, 1995a) and cloud radiative processes, while for anticyclonic anomalies the diabatic processes are commonly believed to be weaker [even though not necessarily inconsequential, e.g., Zierl and Wirth (1997)]. It cannot be excluded that this ''diabatic asymmetry'' results in additional asymmetries concerning the height difference between the thermal and dynamical tropopause, but this question is beyond the scope of the present paper.

Overall we conclude that important differences exist between cyclones and anticyclones regarding their tropopause behavior. Assuming a plausible scenario for the formation of upper-tropospheric anomalies, the dynamics alone can result in significant asymmetries in the height difference between the thermal and the dynamical tropopause. Although there are a number of strong sensitivities, and although other (nondynamical) factors may contribute as well, the good qualitative agreement between our results and the observations of BVR96 suggests that the asymmetries discussed in this paper are relevant in the real atmosphere.

Acknowledgments. The author wants to thank J. Egger and G. Zängl for useful discussions on the subject of this paper. Furthermore, the remarks of an anonymous

referee, which helped to improve the text, are gratefully acknowledged.

REFERENCES

Andrews, D. G., J. R. Holton, and C. B. Leovy, 1987: *Middle Atmosphere Dynamics.* Academic Press, 489 pp.

Beekmann, M., G. Ancellet, and G. Mégie, 1994: Climatology of tropospheric ozone in southern Europe and its relation to potential vorticity. *J. Geophys. Res.,* **99,** 12 841–12 853.

Bethan, S., G. Vaughan, and S. J. Reid, 1996: A comparison of ozone and thermal tropopause heights and the impact of tropopause definition on quantifying the ozone content of the troposphere. *Quart. J. Roy. Meteor. Soc.,* **122,** 929–944.

Danielsen, E. F., 1968: Stratospheric-tropospheric exchange based on radioactivity, ozone and potential vorticity. *J. Atmos. Sci.,* **25,** 502–518.

Defant, F., and H. Taba, 1957: The threefold stucture of the atmosphere and the characteristics of the tropopause. *Tellus,* **9,** 259–274.

Dobson, G. M. B., 1973: The laminated structure of the ozone in the atmosphere. *Quart. J. Roy. Meteor. Soc.,* **99,** 599–607.

Highwood, E., and B. J. Hoskins, 1998: The tropical tropopause. *Quart. J. Roy. Meteor. Soc.,* **124,** 1579–1604.

Holton, J. R., P. H. Haynes, M. E. McIntyre, A. R. Douglass, R. B. Rood, and L. Pfister, 1995: Stratosphere–troposphere exchange. *Rev. Geophys.,* **33,** 403–439.

Hoskins, B. J., M. E. McIntyre, and A. W. Robertson, 1985: On the use and significance of isentropic potential vorticity maps. *Quart. J. Roy. Meteor. Soc.,* **111,** 877–946.

Juckes, M., 1994: Quasigeostrophic dynamics of the tropopause. *J. Atmos. Sci.,* **51,** 2756–2768.

Lerke, S. G., 1999: Auswertung von Ozonsondenprofilen zum Zusammenhang zwischen thermischer und Ozon-Tropopause. Diplomarbeit, Ludwig-Maximilians-Universität München, 89 pp. [Available from Meteorological Institute, Theresienstr. 37, 80333 Munich, Germany.]

Price, J. D., and G. Vaughan, 1993: The potential for stratosphere–troposphere exchange in cut-off-low systems. *Quart. J. Roy. Meteor. Soc.,* **119,** 343–365.

Reid, S. J., and G. Vaughan, 1991: Lamination in ozone profiles in the lower stratosphere. *Quart. J. Roy. Meteor. Soc.,* **117,** 825–844.

Shapiro, M. A., 1980: Turbulent mixing within tropopause folds as a mechanism for the exchange of chemical constituents between the stratosphere and troposphere. *J. Atmos. Sci.,* **37,** 994–1004.

Wirth, V., 1995a: Diabatic heating in an axisymmetric cut-off cyclone and related stratosphere–troposphere exchange. *Quart. J. Roy. Meteor. Soc.,* **121,** 127–147.

——, 1995b: Comments on ''A new formulation of the exchange of mass and trace constituents between the stratosphere and troposphere.'' *J. Atmos. Sci.,* **52,** 2491–2493.

——, 2000: Thermal versus dynamical tropopause in upper tropospheric balanced flow anomalies. *Quart. J. Roy. Meteor. Soc.,* **126,** 299–317.

——, and J. Egger, 1999: Diagnosing extratropical synoptic-scale stratosphere–troposphere exchange: A case study. *Quart. J. Roy. Meteor. Soc.,* **125,** 635–655.

WMO, 1957: Meteorology—A three-dimensional science. *WMO Bull.,* **6** (Oct), 134–138.

——, 1986: Atmospheric ozone 1985. World Meteorological Organization Global Ozone Research and Monitoring Project Rep. 16, Vol. I, WMO, Geneva, Switzerland, 240 pp.

Zierl, B., and V. Wirth, 1997: The influence of radiation on tropopause behavior and stratosphere–troposphere exchange in an upper tropospheric anticyclone. *J. Geophys. Res.,* **102,** 23 883–23 894.